



Modeling and simulation of the decohesion of particulate aggregates in a binding matrix

Decohesion of
particulate
aggregates

T.I. Zohdi and P. Wriggers

*Institut für Baumechanik und Numerische Mechanik, Hannover,
Germany*

79

Keywords *Aggregates, Cohesion*

Abstract *A model for the decohesion of aggregates of suspended particulate material in a binding matrix is developed. In the model cohesive zones which envelop each particle individually are introduced at the particulate/binder interface. During progressive loading, the deterioration of the cohesive zones is initiated if constraints placed on the microstress fields are violated. In order for the material behavior to be energetically admissible, the deterioration of the material at a point is in the form of a reduction of the elasticity tensor's eigenvalues at that point. The material within the cohesive zones deteriorates until the constraints are met. In order to isolate and study the effects of interfacial deterioration, outside of the cohesive zones, the material is unaltered. Mathematical properties of the model, as well as physical restrictions, are discussed. Numerical simulations are performed employing the finite element method to illustrate the approach in three-dimensional applications.*

1. Introduction

A key component to the success of many modern structural designs is the microscopically tailored behavior of a material for a desired macroscopic response. A relatively inexpensive way to obtain macroscopically tailored responses is to modify a base material's properties by the addition of microscopic second phase particulate matter. The resulting new material's microstructure consists of aggregates of randomly distributed particles in a binding matrix (Figure 1). For a structural analyst, the usual quantities of interest are related to the overall mechanical response of the suspensions and the binding matrix. A primary concern in the use of such materials is loss in the structural-scale material performance due to microstructural deterioration resulting from highly distorted microfields arising from property mismatches within the material microstructure. In particular, decohesion of the particulate material from the binder is an important issue. Clearly, if the suspensions decohere, then virtually all of the advantageous aggregate properties are lost. Because of the impossibility of obtaining analytical solutions to models of such systems, numerical simulations must be pursued. The simulation of the progressive decohesion of aggregates of particulates requires approaches amenable to rapid computation. One such possible approach is to employ cohesive zone models, which have recently received a great deal of attention in the literature, although they been widely used over the last 30 years, either in continuum formulations, or directly in finite element algorithms. The usual application of the cohesive zone approach is to represent imperfect bonding by

an elastic layer having a critical stress that is dependent on the deformation at the interface (for representative examples, see Needleman, 1987; 1990a; 1990b; 1992; Corigliano, 1993; Allix *et al.*, 1994; Bolzon and Corigliano, 1997; Ortiz and Pandolfi, 1999; Ruiz *et al.*, 2000). Cohesive zone models have a physical basis. Experimental observations have shown that an interface layer usually forms that differs structurally, and consequently mechanically from the materials on either side of the interface (for details, see Eustathopoulos and Mortensen, 1993; Needleman *et al.*, 1993).

In this work, a cohesive zone type microscale model is developed to describe the decohesion of (multibody) aggregates of suspended particulate material in a binding matrix. In the model, cohesive zones, which envelop each individual particle, are introduced at the particulate/binder interface (Figure 1). During progressive loading, the deterioration of the cohesive zones is initiated if constraints placed on the microstress fields, for example critical levels of dilatational and/or deviatoric stresses, are violated. The material must deteriorate until the constraints are satisfied. Outside of the cohesive zones the material is unaltered. The outline of the presentation is as follows. In section 2, a cohesive zone model is introduced. In section 3, mathematical properties of the model, in particular restrictions, are discussed. In section 4, a computational solution algorithm is developed, based on incremental load stepping, implicit recursive global fixed-point iterations and embedded local Newton iterations. In section 5, three-dimensional numerical simulations are presented. In section 6, concluding remarks are given.

2. A constrained BVP for decohesion

We consider a structure which occupies a bounded domain Ω with a boundary denoted $\partial\Omega$. The body is in static equilibrium under the action of body forces, \mathbf{f} , and surface tractions, \mathbf{t} . The boundary $\partial\Omega = \bar{\Gamma}_u \cup \bar{\Gamma}_t$ consists of a part Γ_u and a part Γ_t on which displacements and tractions are respectively prescribed. Following standard notation, we let $H^1(\Omega)$ denote the usual space of functions with generalized partial derivatives of order ≤ 1 in $L^2(\Omega)$. We define $\mathbf{H}^1(\Omega) \stackrel{\text{def}}{=} [H^1(\Omega)]^3$ as the space of vector-valued functions whose components

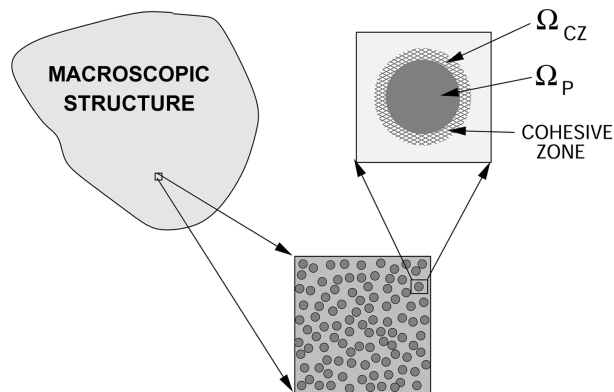


Figure 1.
A macroscopic body made of a material composed of a matrix with additives. Cohesive zones which envelop each particle (cross-section shown)

have generalized partial derivatives of order ≤ 1 in $\mathbf{L}^2(\Omega) \stackrel{\text{def}}{=} [L^2(\Omega)]^3$. We shall use the symbol “ $\mathbf{u}|_{\partial\Omega}$ ”, for example, for boundary values of the displacement. We assume that the loading data are such that $\mathbf{t} \in \mathbf{L}^2(\partial\Omega)$ and $\mathbf{f} \in \mathbf{L}^2(\Omega)$, however, rougher data is possible. The “virgin” (undecohesed) mechanical properties of the heterogeneous material are characterized by a spatially varying elasticity tensor $\mathbf{IE} \in \mathbb{R}^{3^2 \times 3^2}$ which is assumed to satisfy $a_+ \boldsymbol{\epsilon} : \boldsymbol{\epsilon} \geq \boldsymbol{\epsilon} : \mathbf{IE} : \boldsymbol{\epsilon} \geq a_- \boldsymbol{\epsilon} : \boldsymbol{\epsilon}$, $\forall \boldsymbol{\epsilon} \in \mathbb{R}^{3 \times 3}$, $\boldsymbol{\epsilon} = \boldsymbol{\epsilon}^T$, $\infty > a_-, a_+ > 0$, $\forall \mathbf{x} \in \Omega$, where $E_{ijkl}(\mathbf{x}) = E_{jikl}(\mathbf{x}) = E_{ijlk}(\mathbf{x}) = E_{klij}(\mathbf{x})$, $1 \leq i, j, k, l \leq 3$, $E_{ijkl}(\mathbf{x})$ being the Cartesian components of \mathbf{IE} at point \mathbf{x} .

We denote \mathbf{u} as the solution field of the following variational boundary value problem with a linearly elastic material microstructure:

$$\begin{aligned} &\text{Find } \mathbf{u} \in \mathbf{H}^1(\Omega), \mathbf{u}|_{\Gamma_u} = \mathbf{d}, \text{ such that} \\ &\int_{\Omega} \nabla \mathbf{v} : \mathbf{IE} : \nabla \mathbf{u} \, d\Omega \\ &= \int_{\Omega} \mathbf{f} \cdot \mathbf{v} \, d\Omega + \int_{\Gamma_t} \mathbf{t} \cdot \mathbf{v} \, dA \quad \forall \mathbf{v} \in \mathbf{H}^1(\Omega), \mathbf{v}|_{\Gamma_u} = 0. \end{aligned} \quad (1)$$

This formulation contains no description of microscopic deterioration, which we refer to by “relaxation” effects. To describe deterioration of the material on the microscopic level, we construct a relaxed solution, \mathbf{u}_{rel} , that is generated by using a deformation-dependent weakened material modulus, $\mathbf{IE}_{\text{rel}} \leq \mathbf{IE}$. The notation $\mathbf{IE}_{\text{rel}} \leq \mathbf{IE}$ means that the eigenvalues of $\mathbf{IE} - \mathbf{IE}_{\text{rel}}$ are nonnegative. The corresponding variational boundary value problem governing the relaxed solution is:

$$\begin{aligned} &\text{Find } \mathbf{u}_{\text{rel}} \in \mathbf{H}^1(\Omega), \mathbf{u}_{\text{rel}}|_{\Gamma_u} = \mathbf{d}, \text{ such that} \\ &\int_{\Omega} \nabla \mathbf{v} : \mathbf{IE}_{\text{rel}} : \nabla \mathbf{u}_{\text{rel}} \, d\Omega \\ &= \int_{\Omega} \mathbf{f} \cdot \mathbf{v} \, d\Omega + \int_{\Gamma_t} \mathbf{t} \cdot \mathbf{v} \, dA \quad \forall \mathbf{v} \in \mathbf{H}^1(\Omega), \mathbf{v}|_{\Gamma_u} = 0, \end{aligned} \quad (2)$$

If $\mathcal{M} < \mathcal{K}$ then $\mathbf{IE}_{\text{rel}} = \mathbf{IE}$ (no relaxation),
If $\mathcal{M} = \mathcal{K}$ then $\mathbf{0} < \mathbf{IE}_{\text{rel}} \leq \mathbf{IE}$ (relaxation).

The functions $\mathcal{M} = \mathcal{M}(\mathbf{IE}_{\text{rel}}, \mathbf{u}_{\text{rel}})$ and $\mathcal{K} = \mathcal{K}(\mathbf{IE}_{\text{rel}}, \mathbf{u}_{\text{rel}})$, which are scalar functions in present analysis, respectively serve as a measure of, and constraint on, selected internal fields of interest to the analyst. Specific forms will be given in the next section. For energetic reasons, a sufficient way to meet our physical restrictions, is to force the eigenvalues of \mathbf{IE}_{rel} to decrease at a location where deterioration occurs, and to remain constant otherwise. This ensures for a weakening body undergoing irreversible changes that:

- (1) under pure displacement boundary loading control, $\Gamma_u = \partial\Omega$, the body should exhibit energy dissipation; and

- (2) for pure traction loading control, $\Gamma_t = \partial\Omega$, the body should exhibit an energy increase.

To see this, consider two symmetric positive definite material property (elasticity tensor) distributions, the unrelaxed material, \mathbf{IE} , and a deteriorated or relaxed material \mathbf{IE}_{rel} . Both are separately used to generate solutions to two boundary value problems, with different material coefficients, but having the same exterior geometry and loading. The corresponding displacement (\mathbf{u}), stress ($\boldsymbol{\sigma}$) and strain ($\boldsymbol{\epsilon} = \frac{1}{2}(\nabla\mathbf{u} + (\nabla\mathbf{u})^T)$) states produced when using these materials are denoted $(\mathbf{u}, \boldsymbol{\sigma}, \boldsymbol{\epsilon})$ and $(\mathbf{u}_{\text{rel}}, \boldsymbol{\sigma}_{\text{rel}}, \boldsymbol{\epsilon}_{\text{rel}})$ respectively. Defining their respective strain energies by:

$$\Pi \stackrel{\text{def}}{=} \underbrace{\int_{\Omega} \boldsymbol{\epsilon} : \mathbf{IE} : \boldsymbol{\epsilon} d\Omega}_{\text{unrelaxed energy}} \quad \text{and} \quad \Pi_{\text{rel}} \stackrel{\text{def}}{=} \underbrace{\int_{\Omega} \boldsymbol{\epsilon}_{\text{rel}} : \mathbf{IE}_{\text{rel}} : \boldsymbol{\epsilon}_{\text{rel}} d\Omega}_{\text{relaxed energy}}, \quad (3)$$

we have the following result for $\Gamma_u = \partial\Omega$:

$$(\mathbf{IE} - \mathbf{IE}_{\text{rel}}) \geq \mathbf{0} \Rightarrow \underbrace{\int_{\Omega} \boldsymbol{\epsilon} : \mathbf{IE} : \boldsymbol{\epsilon} d\Omega}_{\Pi} - \underbrace{\int_{\Omega} \boldsymbol{\epsilon}_{\text{rel}} : \mathbf{IE}_{\text{rel}} : \boldsymbol{\epsilon}_{\text{rel}} d\Omega}_{\Pi_{\text{rel}}} \geq 0. \quad (4)$$

Similarly, defining:

$$\Pi \stackrel{\text{def}}{=} \underbrace{\int_{\Omega} \boldsymbol{\sigma} : \mathbf{IE}^{-1} : \boldsymbol{\sigma} d\Omega}_{\text{unrelaxed energy}} \quad \text{and} \quad \Pi_{\text{rel}} \stackrel{\text{def}}{=} \underbrace{\int_{\Omega} \boldsymbol{\sigma}_{\text{rel}} : \mathbf{IE}_{\text{rel}}^{-1} : \boldsymbol{\sigma}_{\text{rel}} d\Omega}_{\text{relaxed energy}}, \quad (5)$$

we have $\delta\boldsymbol{\sigma} = \boldsymbol{\sigma}_{\text{rel}} - \boldsymbol{\sigma}$, if $\Gamma_t = \partial\Omega$:

$$\begin{aligned} (\mathbf{IE}^{-1} - \mathbf{IE}_{\text{rel}}^{-1}) < \mathbf{0} \Rightarrow & \underbrace{\int_{\Omega} \boldsymbol{\sigma} : \mathbf{IE}^{-1} : \boldsymbol{\sigma} d\Omega}_{\Pi} \\ & - \underbrace{\int_{\Omega} \boldsymbol{\sigma}_{\text{rel}} : \mathbf{IE}_{\text{rel}}^{-1} : \boldsymbol{\sigma}_{\text{rel}} d\Omega}_{\Pi_{\text{rel}}} \leq 0. \end{aligned} \quad (6)$$

The relations in equations (4) and (6) provide sufficient restrictions on the properties of a relaxed microstructure such that physically realistic macroscopic responses can be ensured (for proofs, see Zohdi and Wriggers, forthcoming; Huet *et al.*, 1991; for related material/energy ordering theorems, see Hill, 1963). In the simplest case, one can define a spatially varying scalar relaxation function, α , such that $\mathbf{IE}_{\text{rel}} = \alpha\mathbf{IE}$ with $0 < \alpha \leq 1$, $\forall \mathbf{x} \in \Omega$. The scalar function α takes on different values throughout the body, which are dictated by the solution to the relaxed boundary value problem. When the

material is isotropic (two free constants), we have $\mathbf{IE} : \boldsymbol{\epsilon} = 3\kappa \frac{tr\boldsymbol{\epsilon}}{3} \mathbf{I} + 2\mu \boldsymbol{\epsilon}'$, where $tr\boldsymbol{\epsilon} = \epsilon_{ii}$ and $\boldsymbol{\epsilon}' = \boldsymbol{\epsilon} - \frac{1}{3}(tr\boldsymbol{\epsilon})\mathbf{I}$. The eigenvalues of an isotropic elasticity tensor are $(3\kappa, 2\mu, 2\mu, \mu, \mu, \mu)$. Therefore, we must have $\alpha\kappa > 0$ and $\alpha\mu > 0$ to retain positive definiteness of \mathbf{IE}_{rel} .

An important observation is that one can restrict the relaxation to “zones of interest”. In this work the zones of interest are the interfacial cohesive zones between materials. To model three dimensional cohesive zones requires the restriction of the general relaxation formulation to cohesive zones enveloping the particles (Figure 1). The domain of a cohesive zone, Ω_{CZ} , is defined via $\Omega_{CZ} \stackrel{\text{def}}{=} \Omega_{P+\delta P} - \Omega_P$, where $\Omega_{P+\delta P}$ is a dilated form of Ω_P . In order to isolate and study the effects of decohesion, outside of the cohesive zone the material is unaltered. In summary, in order to solve the boundary value problem, we must find a solution \mathbf{u}_{rel} , and a function α , such that the constraints and equilibrium are satisfied simultaneously. To accomplish this, later in the work we construct global/local iteration procedures in conjunction within an incremental load stepping scheme.

3. Constraint forms

As stated in the previous section, the values of α are dictated by the fact that the solution \mathbf{u}_{rel} must satisfy the equations of equilibrium, and simultaneously the constraints. Algorithmically, when the constraint is violated during loading we must enforce:

$$\Lambda(\alpha) \stackrel{\text{def}}{=} \mathcal{M}(\boldsymbol{\sigma}(\alpha)) - \mathcal{K}(\alpha) = 0. \quad (7)$$

A relatively general set of functions are:

$$\mathcal{M}(\boldsymbol{\sigma}_{rel}(\alpha)) = (g(\boldsymbol{\sigma}_{rel}(\alpha)) : g(\boldsymbol{\sigma}_{rel}(\alpha)))^{\frac{1}{2}}$$

and:

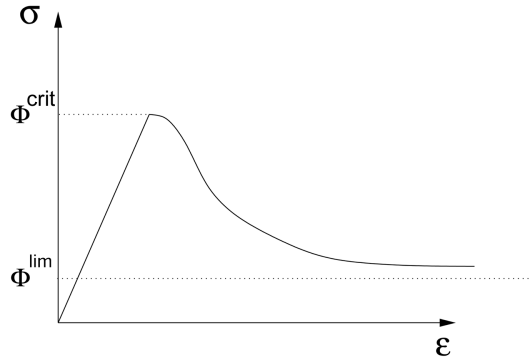
$$\mathcal{K}(\alpha) \stackrel{\text{def}}{=} \Phi^{lim} + (\Phi^{crit} - \Phi^{lim})\alpha^P$$

where:

$$g(\boldsymbol{\sigma}_{rel}) = \eta_1 \frac{tr\boldsymbol{\sigma}_{rel}}{3} \mathbf{I} + \eta_2 (\boldsymbol{\sigma}_{rel} - \frac{tr\boldsymbol{\sigma}_{rel}}{3} \mathbf{I}), \quad (8)$$

and where η_1 and η_2 are positive weights (different for each constituent material) which reflect the type of deterioration mechanism, hydrostatic and/or deviatoric, to be expected. The material parameters Φ^{crit} and Φ^{lim} (different for each component material) are analogous to critical and limit levels of stress (Figure 2). There are restrictions on the material constants in the constraint form for the relaxed boundary value problem to be well-posed, i.e. solvable. This is discussed next.

Figure 2.
The meaning of the terms in the relaxation function



3.1 A dissipation inequality

For any closed cycle there must be energy dissipated during relaxation. Therefore, for any subvolume ω contained in the body Ω we have:

$$\int_0^T \int_{\omega} \boldsymbol{\sigma}_{rel} : \dot{\boldsymbol{\epsilon}}_{rel} d\omega dt \geq 0, \tag{9}$$

where $(0, T)$ is the time duration for the closed loading cycle. However, since the loading cycle and ω are arbitrary, $\boldsymbol{\sigma}_{rel} : \dot{\boldsymbol{\epsilon}}_{rel} \geq 0$ always holds. The equality can be attained only when no relaxation occurs. In one dimension, the restriction is depicted in Figure 3. As an example, consider a one-dimensional bar composed of a material that is initially linearly-elastic. For a displacement tension test load: $u_{rel}(0) = 0$ and $u_{rel}(x = L) = \mathcal{E} \times L$, where \mathcal{E} is an arbitrary positive constant that represents “applied strain”. The corresponding boundary value problem is:

$$\frac{d}{dx} \left(E_{rel} \frac{du_{rel}}{dx} \right) = 0 \Rightarrow \frac{du_{rel}}{dx} = \mathcal{E} \Rightarrow \sigma_{rel} = E_{rel} \mathcal{E}, \tag{10}$$

where $E_{rel} = \alpha E$ is a material which may relax (Figure 4). Consider the one dimensional constraint analog to equation (7):

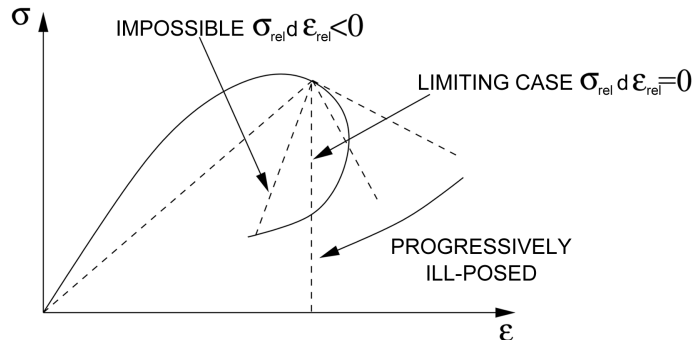


Figure 3.
A dissipation inequality for relaxation

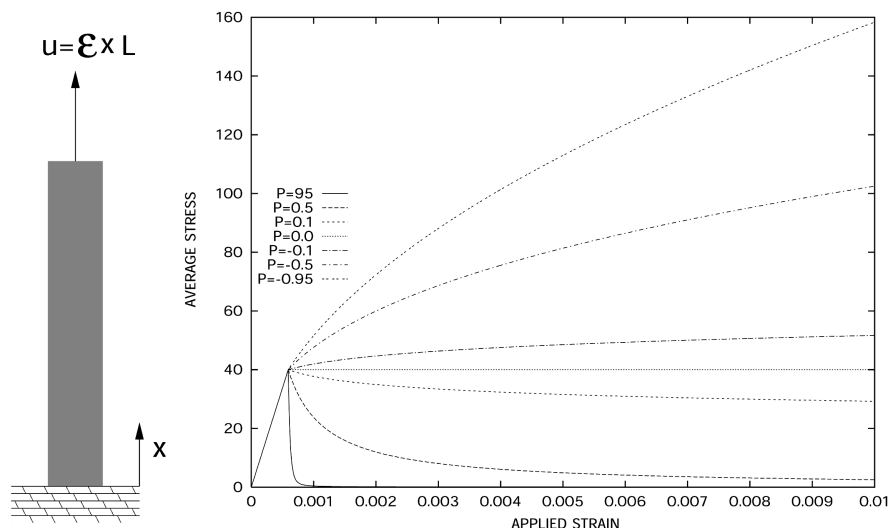


Figure 4.
One-dimensional bar
under displacement
control: a parameter
study for a single
material with
 $\sigma^{lim} \ll \sigma_0^{crit} = 40\text{MPa}$,
 $E = 67.5\text{GPa}$

$$\Lambda = \sigma_{rel} - (\sigma^{lim} + (\sigma_0^{crit} - \sigma^{lim})\alpha^P) = 0. \quad (11)$$

For certain choices of σ^{lim} , σ_0^{crit} and P , this problem can be ill-posed. To illustrate this, consider $\sigma^{lim} = 0$ and $P = 1$, which leads to:

$$\Lambda = \sigma_{rel} - (\sigma_0^{crit} - \sigma^{lim})\alpha^P = 0 \Rightarrow \alpha(E\epsilon - \sigma^{crit}) = 0. \quad (12)$$

For this equation to have a solution, either $\sigma_0^{crit} = E\epsilon_{rel}$ or $\alpha = 0$ (which is inadmissible). However, under displacement control $\epsilon_{rel} = \epsilon$, which implies for a fixed σ_0^{crit} , and a changing ϵ_{rel} , that $\sigma_0^{crit} \neq E\epsilon_{rel}$, therefore forcing $\alpha = 0$. This implies $\sigma_{rel}d\epsilon_{rel} = 0$, which violates the dissipation inequality, as well as the restriction that $E_{rel} = \alpha E$ be positive. Therefore the constraints cannot be satisfied. Figure 4 shows the response of a one dimensional (aluminum) bar, where the critical stress has been taken to be the yield stress, for various values of P . To generate the solution 1,000 load increments were used, and Newton's method was employed to solve the system within each load increment. Clearly, as $P \rightarrow 1$, the boundary value problem becomes unsolvable.

4. Three-dimensional computational solution procedure

For three-dimensional computations, we employ an incremental load stepping scheme and a recursive global fixed-point algorithm containing (local) internal Newton iterations. Within a load step the basic philosophy is:

- (1) a global trial solution state is computed, ignoring the constraints;
- (2) the constraint violations are checked throughout the domain;
- (3) in locations where the constraints are not satisfied, relaxation is activated, in the form of material stiffness reductions computed by a local Newton algorithm; and

- (4) the global equilibrium equations are then resolved with the new predicted relaxation distribution.

The procedure is then repeated until a tolerance is met on the constraints. This is combined with an incremental load stepping procedure, where steps (1)-(4) are applied within each load step.

We employ the following hierarchical superscript notation:

- L is the load increment counter;
- I is the global solve counter (within a load increment); and
- i is the local internal Newton iteration counter (within a global solve).

During the incremental load stepping procedure, it is assumed that the stress $\boldsymbol{\sigma}_{\text{rel}}^{(L-1, \cdot, \cdot)}$ and the relaxation $\alpha^{(L-1, \cdot, \cdot)}$ have been determined to sufficient accuracy that $\Lambda(\boldsymbol{\sigma}_{\text{rel}}^{(L-1, \cdot, \cdot)}, \alpha^{(L-1, \cdot, \cdot)}) \leq \text{tol}, \forall \mathbf{x} \in \Omega$, at loading level $L - 1$. Now the external load is incremented, and it is initially assumed that the internal fields produce no increased relaxation:

$$\begin{aligned} &\text{Find } \mathbf{u}_{\text{rel}}^{(L)} \in \mathbf{H}^1(\Omega), \mathbf{u}_{\text{rel}}^{(L)}|_{\Gamma_u} = \mathbf{d}^{(L)}, \text{ such that } \forall \mathbf{v} \in \mathbf{H}^1(\Omega), \mathbf{v}|_{\Gamma_u} = 0. \\ &\int_{\Omega} \nabla \mathbf{v} : \boldsymbol{\sigma}_{\text{rel}}^{(L)} d\Omega = \int_{\Omega} \mathbf{f}^{(L)} \cdot \mathbf{v} d\Omega + \int_{\Gamma_t} \mathbf{t}^{(L)} \cdot \mathbf{v} dA, \\ &\boldsymbol{\sigma}_{\text{rel}}^{(L)} = \boldsymbol{\sigma}_{\text{rel}}^{(L, \cdot, \cdot)} \stackrel{\text{def}}{=} \alpha^{(L-1, \cdot, \cdot)} \mathbf{I} \mathbf{E} : \boldsymbol{\epsilon}_{\text{rel}}^{(L, \cdot, \cdot)}, \end{aligned} \quad (13)$$

where the current (incrementally applied loads) load values are $\mathbf{f}^{(L)}, \mathbf{t}^{(L)}$ and $\mathbf{d}^{(L)}$. If $\Lambda(\boldsymbol{\sigma}_{\text{rel}}^{(L, \cdot, \cdot)}, \alpha^{(L, \cdot, \cdot)}) \leq \text{tol}, \forall \mathbf{x} \in \Omega$, then the ‘‘predictor’’ is assumed correct. If $\Lambda(\boldsymbol{\sigma}_{\text{rel}}^{(L, \cdot, \cdot)}, \alpha^{(L, \cdot, \cdot)}) > \text{tol}, \forall \mathbf{x} \in \Omega$, then some relaxation has occurred and must be determined. Following the usual procedure for problems with constraints, within a load increment L , a global solution is computed for equilibrium, and a Newton-Raphson scheme is used to satisfy the constraints locally. The displacement field, and consequently the strain field, are frozen during these local iterations. The local constraint can be written as $(\boldsymbol{\sigma}_{\text{rel}}^{L, I, i} = \alpha^{L, I, i} \mathbf{I} \mathbf{E} : \boldsymbol{\epsilon}_{\text{rel}}^{L, I, i})$:

$$\begin{aligned} \Lambda(\alpha^{L, I, i} + \Delta \alpha^{L, I, i}) &= \Lambda(\alpha^{L, I, i}) + \frac{\partial \Lambda}{\partial \alpha} \Big|_{\alpha^{L, I, i}} \Delta \alpha^{L, I, i} \\ &+ \text{higher order terms} = 0. \end{aligned} \quad (14)$$

This leads to:

$$\alpha^{L, I, i+1} = \alpha^{L, I, i} - \frac{\Lambda(\alpha^{L, I, i})}{\frac{\partial \Lambda}{\partial \alpha} \Big|_{\alpha^{L, I, i}}}. \quad (15)$$

This is locally iterated until the constraints are satisfied to a tolerance. The global problem is then resolved, with the updated relaxed state. After the global resolve, the constraints are then locally checked, and the relaxation

updated if necessary, again by freezing the globally updated strains and employing the local Newton scheme.

4.1 A global/local solution algorithm

In the algorithm to follow, within each load increment, the (global/local) system is recursively resolved until the constraints and equilibrium are satisfied. The chosen global measure to determine the violation of the constraints is:

$$\|\mathcal{M} - \mathcal{K}\|_C \stackrel{\text{def}}{=} \frac{1}{|\Omega|} \int_{\Omega} \frac{\max(\mathcal{M}, \mathcal{K}) - \mathcal{K}}{\mathcal{K}} d\Omega. \quad (16)$$

The algorithm is as follows, for example, for incremental displacement control:

$L = 1, \alpha^L = 1 \forall \mathbf{x} \in \Omega_{CZ}$ (COHESIVE ZONES)

- (1) INCREMENT LOAD : $\mathbf{u}_{\text{rel}}^L|_{\Gamma_u} \stackrel{\text{def}}{=} \mathbf{u}_{\text{rel}}^{L-1}|_{\Gamma_u} + \delta \mathbf{u}_{\text{rel}}^L|_{\Gamma_u}, I = 1$
 - (2) GLOBALLY COMPUTE $\mathbf{u}_{\text{rel}}^{L,I}$ AND $\gamma^{L,I} \stackrel{\text{def}}{=} \|\mathcal{M}^{L,I} - \mathcal{K}^{L,I}\|_C$
- FLAG = 0
- IF ($\gamma^{L,I} > \text{TOL}$) THEN
- FLAG = 1
- ENDIF
- FOR EACH $\mathbf{x} \in \Omega_{CZ}$:
- IF ($\mathcal{M}^{L,I} > \mathcal{K}^{L,I}$) THEN
- UPDATE $\alpha^{L,I,i}$ UNTIL $\Lambda(\alpha^{L,I,i}) = 0$
- ENDIF
- $\forall \mathbf{x} \in \Omega_{CZ}$ UPDATE $\alpha^{L,I}$ AND $\mathbf{IE}^{L,I}; I = I + 1$
- IF (FLAG = 1) THEN
- GOTO (2)
- ENDIF
- $L = L + 1$ AND GOTO (1)

5. Three-dimensional cohesive zone simulations

In solid mechanics, the classical goal has usually been to determine a relation between averages, a so-called “effective” property, which is a macroscopic scale linear elasticity tensor, \mathbf{IE}^* , defined via $\langle \boldsymbol{\sigma} \rangle_{\Omega} = \mathbf{IE}^* : \langle \boldsymbol{\epsilon} \rangle_{\Omega}$, where $\langle \cdot \rangle_{\Omega} \stackrel{\text{def}}{=} \frac{1}{|\Omega|} \int_{\Omega} \cdot d\Omega$, and where $\boldsymbol{\sigma}$ and $\boldsymbol{\epsilon}$ are the stress and strain tensor fields within a statistically representative volume element (RVE) with volume $|\Omega|$. Accordingly, examples focus on simulating the relationship between $\langle \boldsymbol{\sigma}_{\text{rel}} \rangle_{\Omega}$ vs $\langle \boldsymbol{\epsilon}_{\text{rel}} \rangle_{\Omega}$ during progressive decohesion.

5.1 Preliminary tests

In linear elasticity, a compact micro/macro energy equivalence statement, $\langle \boldsymbol{\sigma} : \boldsymbol{\epsilon} \rangle_{\Omega} = \langle \boldsymbol{\sigma} \rangle_{\Omega} : \langle \boldsymbol{\epsilon} \rangle_{\Omega}$, known as Hill's condition (Hill, 1952), dictates the size requirements placed on the RVE. This macro/micro energy condition must be realizable by the fields within the RVE for the sample to admit to an energetically sensible homogenization in the linearly elastic range. For any perfectly bonded heterogeneous body, in the absence of body forces, two physically important loading states satisfy Hill's condition. They are (with $\mathbf{f} = 0$):

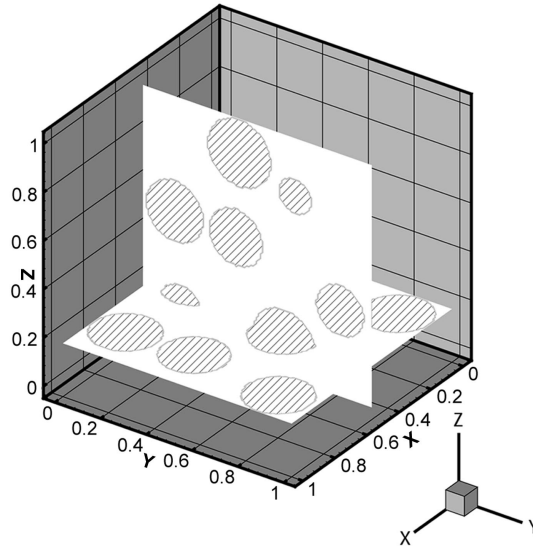
- (1) pure linear displacements of the form $\mathbf{u}|_{\partial\Omega} = \mathcal{E} \cdot \mathbf{x} \Rightarrow \langle \boldsymbol{\epsilon} \rangle_{\Omega} = \mathcal{E}$; or
- (2) pure tractions in the form $\mathbf{t}|_{\partial\Omega} = \mathcal{L} \cdot \mathbf{n} \Rightarrow \langle \boldsymbol{\sigma} \rangle_{\Omega} = \mathcal{L}$, where \mathcal{E} and \mathcal{L} are constant strain and stress tensors, respectively.

Clearly, for Hill's conditions to be satisfied within a macroscopic body under nonuniform external (engineering) loading, the sample must be large enough to have relatively small boundary field fluctuations relative to its size. Therefore applying the mentioned type of boundary conditions to a large sample is a possible way of reproducing approximately what may be occurring in a statistically representative microscopic sample of material in a macroscopic body. If the effective response is assumed isotropic then only one test loading (instead of usually six) containing non-zero dilatational ($\frac{tr\boldsymbol{\sigma}}{3}$ and $\frac{tr\boldsymbol{\epsilon}}{3}$) and deviatoric components ($\boldsymbol{\sigma}' \stackrel{\text{def}}{=} \boldsymbol{\sigma} - \frac{tr\boldsymbol{\sigma}}{3}\mathbf{I}$ and $\boldsymbol{\epsilon}' \stackrel{\text{def}}{=} \boldsymbol{\epsilon} - \frac{tr\boldsymbol{\epsilon}}{3}\mathbf{I}$), is necessary to determine the effective bulk and shear moduli:

$$3\kappa^* \stackrel{\text{def}}{=} \frac{\langle \frac{tr\boldsymbol{\sigma}}{3} \rangle_{\Omega}}{\langle \frac{tr\boldsymbol{\epsilon}}{3} \rangle_{\Omega}} \quad \text{and} \quad 2\mu^* \stackrel{\text{def}}{=} \sqrt{\frac{\langle \boldsymbol{\sigma}' \rangle_{\Omega} : \langle \boldsymbol{\sigma}' \rangle_{\Omega}}{\langle \boldsymbol{\epsilon}' \rangle_{\Omega} : \langle \boldsymbol{\epsilon}' \rangle_{\Omega}}}. \quad (18)$$

It is clear that even if the responses are not purely isotropic, the relations in equation (18) can be interpreted as generalized effective isotropic moduli.

In order to obtain a rough idea for the size of a statistically representative element, in a preliminary set of tests in the linear elastic range, we considered a smooth microstructural idealization, i.e. embedded spherical particles in a homogeneous matrix. The matrix material was an aluminum ($(\kappa, \mu) = (77.9, 24.9)$ GPa) matrix containing N spherical nonintersecting boron ($(\kappa, \mu) = (230, 172)$ GPa) particles randomly distributed throughout a unit cube (cross-sections shown in Figure 5). This material combination is representative of the typical mismatches in industrially used metal matrix dispersed particulate materials. We controlled the amount of embedded boron via particle/sample size ratio. We defined a subvolume size $V \stackrel{\text{def}}{=} \frac{L \times L \times L}{N}$, where N is the number of particles in the entire sample and where L is the length of the (cubic $L \times L \times L$) sample. A generalized diameter was defined, d , which was the diameter of the smallest sphere that can enclose a single particle of possibly non-spherical shape, although in this work we restricted ourselves to spherical shapes. The ratio between the generalized diameter and the subvolume was a control parameter defined by $\zeta \stackrel{\text{def}}{=} \frac{d}{V^{1/3}}$. The finite element meshes were repeatedly refined, and a mesh density of $9 \times 9 \times 9$ trilinear hexahedra (approximately 2,200-3,000



Mutually orthogonal cross-sections of the geometry as seen by the mesh resolution used for a twenty particle microstructure. Randomly dispersed particulate matter. The hatched areas represent boron and white represents aluminium.

Figure 5.
Mutually orthogonal
cross-sections of the
geometry

degrees of freedom (DoF) per particle was found to deliver invariant macroscopic responses. A “2/5” Gauss rule was used, whereby element with discontinuities had increased Gauss rules ($5 \times 5 \times 5$) to increase the resolution of the internal geometry, while elements with no discontinuities had the nominal $2 \times 2 \times 2$ rule. Detailed theoretical and numerical studies of such processes can be found in Zohdi *et al.* (1998).

The number of particles contained in a sample were increased holding the volume fraction constant. The (uniform multiaxial) loading was $\mathbf{u}|_{\partial\Omega} = \mathcal{E} \cdot \mathbf{x}$, where $\mathcal{E}_{ij} = 0.001$, $i, j = 1, 2, 3$, where \mathbf{x} is a position vector to the boundary of the cube. The following particle per sample sequence was used: 2 (5,184 DoF), 4 (10,125 DoF), 8 (20,577 DoF), 16 (41,720 DoF), 32 (81,000 DoF) and 64 (151,959 DoF) particles. The dimensions of the particles were controlled by setting $\zeta = 0.75$. This resulted in a particulate volume fraction of approximately 22 percent. Five tests were performed at each sample/particulate size ratio level (each with a different random distribution), and the results averaged (Figure 6). At each size ratio level the samples had the same volume fraction. The difference between successive effective moduli were less than 1 percent for samples containing above 20 particles. With this somewhat *ad hoc* justification, we used 20 particle microstructures in the incremental decohesion simulations to follow.

5.2 Incremental decohesion simulations

The properties of the cohesive zones were varied between those of aluminum and those of boron by varying the following weighting ($0 \leq \theta \leq 1$):

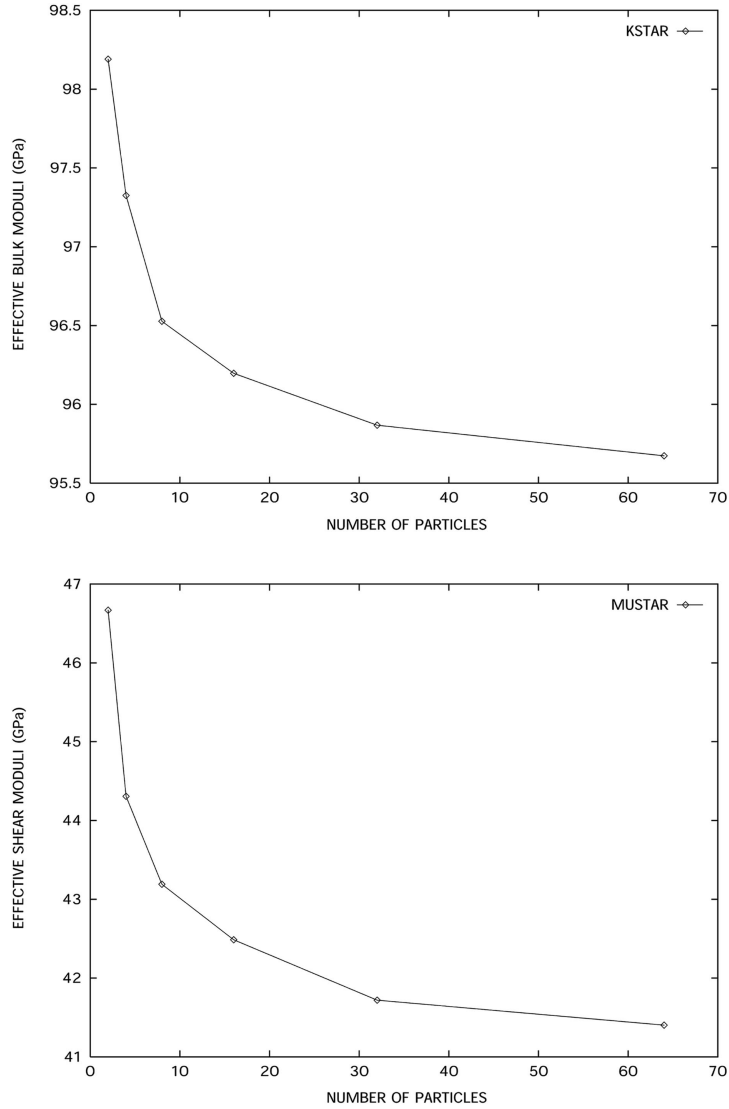


Figure 6.
The values of the effective bulk and shear responses of the system for samples containing various numbers of particles

The values of the effective bulk and shear responses of the system for samples containing various numbers of particles. Five tests were performed per particle/sample size ratio and the results averaged.

$$\begin{aligned}
 (\kappa, \mu, \Phi_{dil}^{crit}, \Phi_{dev}^{crit}) &= \theta(\kappa, \mu, \Phi_{dil}^{crit}, \Phi_{dev}^{crit})|_{\text{PARTICLE}} \\
 &+ (1 - \theta)(\kappa, \mu, \Phi_{dil}^{crit}, \Phi_{dev}^{crit})|_{\text{MATRIX}},
 \end{aligned}
 \tag{19}$$

where, for the constraint function in equation (7):

$$\Phi^{crit} \stackrel{\text{def}}{=} \sqrt{\eta_1^2 (\Phi_{dil}^{crit})^2 + \eta_2^2 (\Phi_{dev}^{crit})^2},$$

and $\Phi^{lim} = \beta\% \times \Phi^{crit}$, where:

- for aluminum, $(\Phi_{dil}^{crit}, \Phi_{dev}^{crit}) = ((80, 40) \text{ MPa})$; and
- for boron, $(\Phi_{dil}^{crit}, \Phi_{dev}^{crit}) = ((1,000, 1,000) \text{ MPa})$.

The case where $\theta = 1$ the cohesive zone had the properties of the particle, and when $\theta = 0$, that of the matrix. We chose the limit stress value to be 1 percent of the critical value, i.e. $\beta\% = 1\%$, to describe near complete decohesion. Throughout the numerical experiments, we used $\eta_1 = \eta_2 = 1$ and $P_\sigma = 0.95$. The cohesive zone thicknesses were taken to be kr , where r is the radius of the particle. Various cohesive zone thicknesses were simulated in the range of $0.05 \leq k \leq 0.3$. For the sake of brevity of presentation of results, we discuss the representative case of $k = 0.2$. All numerical experiments were carried out on a single standard IBM RISC 6000 high performance workstation, and thus the simulations are easily reproducible for other parameter selections.

During the decohesion simulations, if the constraint equation (7) was violated for $\mathbf{x} \in \Omega_{CZ}$, then relaxation was initiated. The load step size was set to 40 displacement-controlled load increments to guide the following displacement-controlled boundary loading history, $\mathbf{u}|_{\partial\Omega} = \mathcal{E}^{begin} \cdot \mathbf{x} \rightarrow \mathcal{E}^{final} \cdot \mathbf{x}$. Multiaxial incremental loading was performed such that $\mathcal{E}_{ij}^{begin} = 0.00$ and $\mathcal{E}_{ij}^{final} = 0.005$. The normalized tolerance on the overall constraint violation in equation (17) was set to $\gamma \leq 0.0001 = \text{tol}$. At this load step size, in all cases, there was no problem with algorithmic convergence. The finite element meshes were repeatedly (uniformly) refined until the responses were invariant. A mesh density of $24 \times 24 \times 24$ trilinear hexahedra ($9 \times 9 \times 9$ per particle) for a total of 46,875 DoF (2,344 per particle), delivered invariant responses throughout the simulations. As in the previous (linearly elastic) numerical experiments, a “2/5” Gauss rule was used. Iterative solvers (Conjugate Gradient) were employed, which allowed the use of the previous increment’s solution as the starting Gauss vector for the next increment. Therefore the computations were relatively fast, with an entire load history taking no more than one hour.

Various cohesive zone properties were used: $\theta = 0.0$, $\theta = 0.2$, $\theta = 0.4$, $\theta = 0.6$, $\theta = 0.8$ and $\theta = 1.0$. In the simulations initially linear responses occurred, which were relatively stiff due to the unrelaxed interfaces, i.e. the “bond” was still intact (Figure 7). Thereafter, a transition period occurred where the cohesive zones heavily relaxed (Figure 8). Such curves are typical for heterogeneous material undergoing decohesion. It is important to note that the nonmonotonicity is to be expected, since the tangent modulus is composed of two “competing” parts:

$$\boldsymbol{\sigma}_{rel} = \alpha \mathbf{IE} : \boldsymbol{\epsilon}_{rel} \Rightarrow d\boldsymbol{\sigma}_{rel} = d\alpha \mathbf{IE} : \boldsymbol{\epsilon}_{rel} + \alpha \mathbf{IE} : d\boldsymbol{\epsilon}_{rel} \stackrel{\text{def}}{=} \mathbf{IE}_{rel}^{\text{TAN}} : d\boldsymbol{\epsilon}_{rel}, \quad (20)$$

where $d\alpha \leq 0$. Essentially, the first term can dominate the second when

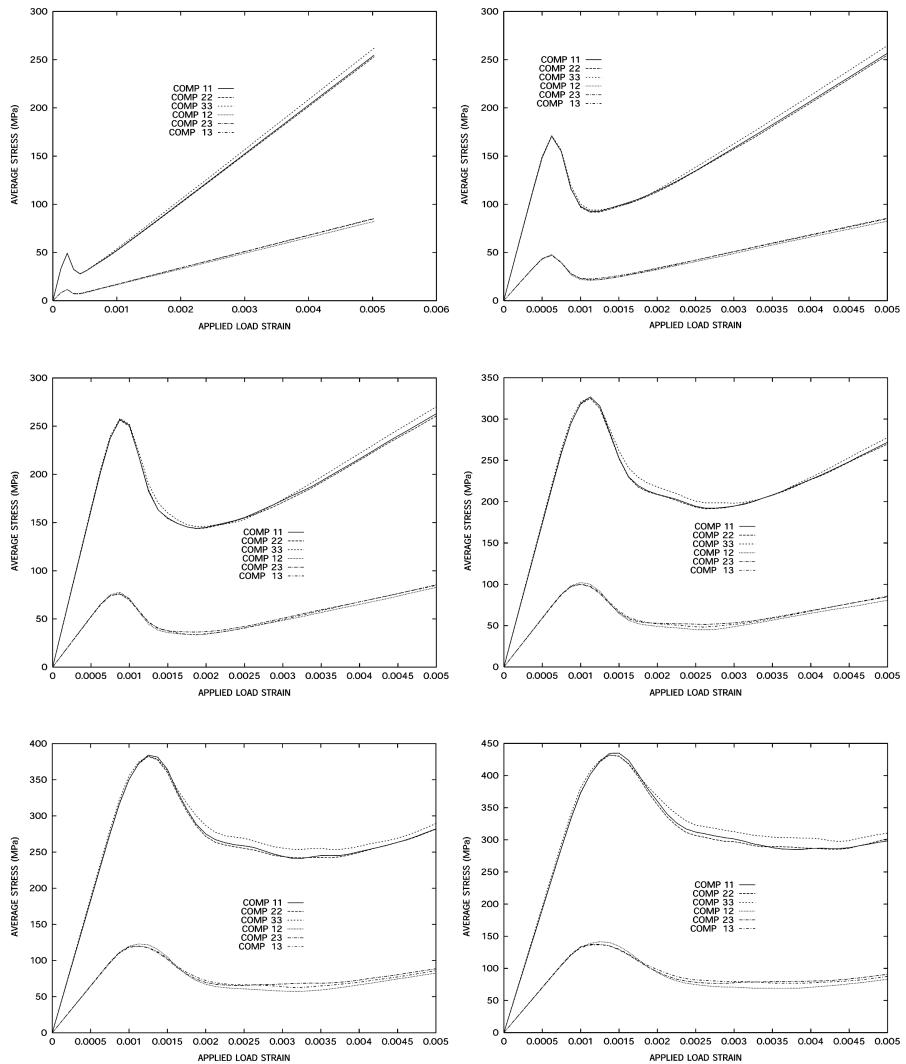


Figure 7.
The stress strain relations for 20 random decohering particles. Left to right, and top to bottom: $\theta = 0.0$, $\theta = 0.2$, $\theta = 0.4$, $\theta = 0.6$, $\theta = 0.8$ and $\theta = 1.0$

the magnitude of $d\alpha$ is large (negative), forcing the tangent response stiffness not to remain positive definite throughout the loading (Figure 8). Figure 9 shows a sequence of slices, with the average values of α per finite element depicted throughout the microstructure, with increasing loading. One clearly sees the progressive evolution of the decohesion around the suspensions.

6. Summary and concluding remarks

In this work we have formulated a micromechanical model to describe the reduction of the overall mechanical stiffness of microheterogeneous material

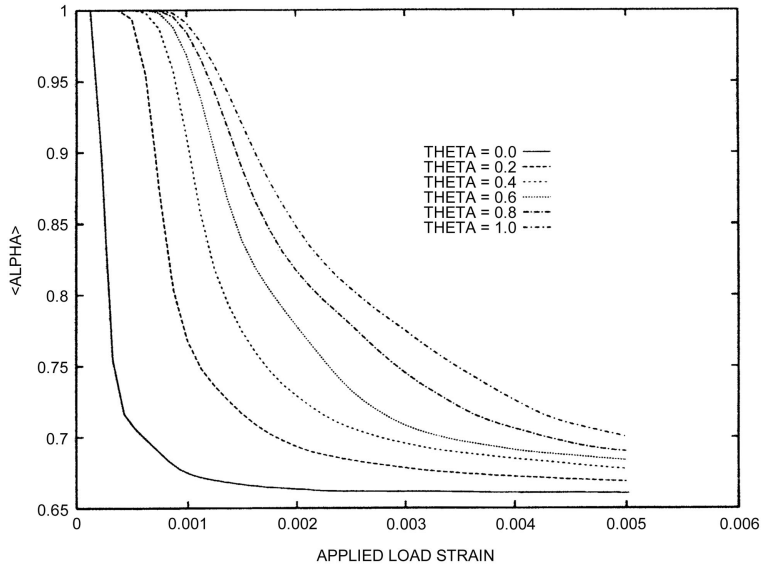


Figure 8.
The $\langle \alpha \rangle_{\Omega}$ vs. applied strain for 20 random particles for various cohesive zone properties and strengths controlled by $\theta = 0.0$, $\theta = 0.2$, $\theta = 0.4$, $\theta = 0.6$, $\theta = 0.8$ and $\theta = 1.0$

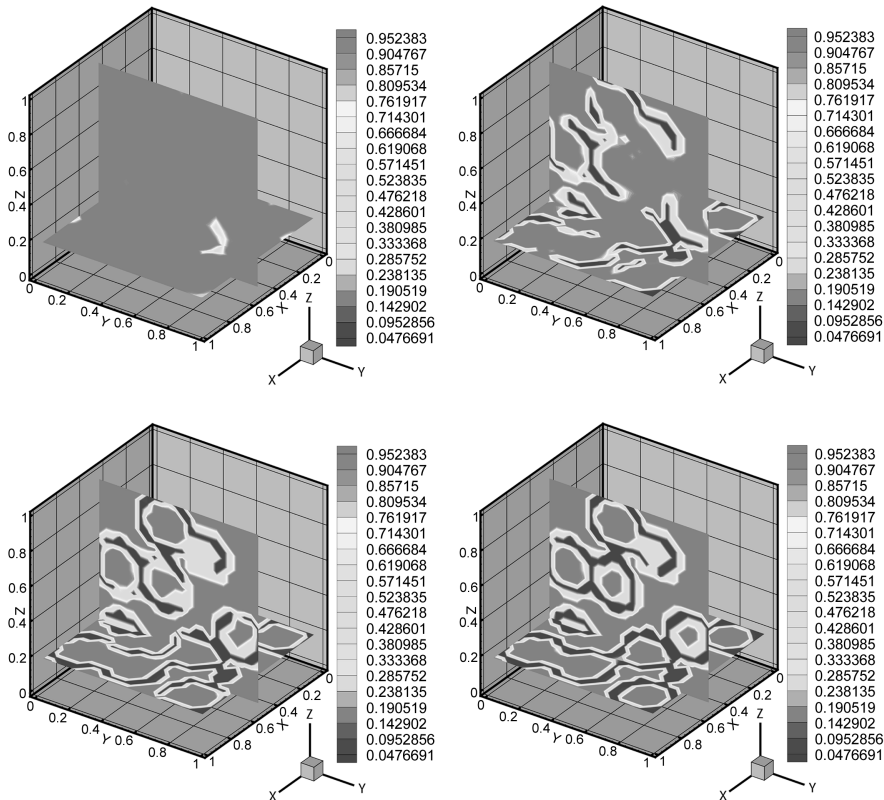


Figure 9.
Mutually orthogonal cross-sections of the decohesion (distribution of α) in a 20 particle microstructure after five, ten, 20 and 40 increments for $\theta = 0.4$. The depicted values of α were averaged over each finite element

specimens due to the decohesion of suspensions. The effects of local microscopic deterioration were modeled by a variational boundary value problem with constraints on the microfields. In the model, in order to satisfy the constraints, the original material had to relax on the microstructural level. Mathematically this was achieved by reducing the eigenvalues of the elasticity tensor at points within cohesive zones. A global fixed point algorithm, in conjunction with local Newton iterations, was used within an incremental load stepping scheme to solve the microdecohesion problem. Three-dimensional responses of aggregates of suspended additive particulate matter were simulated by direct finite element techniques to illustrate the approach.

An issue which we are currently investigating is: "What should be added to a base matrix to achieve a prespecified macroscopic response, with minimal losses due to decohesion?" Such inverse problems of optimization of microstructure possess associated nonconvex objective functions. In other words, there are multiple local design minima. Finding the global minimum of highly nonconvex functions is not trivial, and in general one must restart the search from different initial guesses to locate other local potential minima. There are a variety of ways in which to accelerate such searches. In the literature, methods such as simulated annealing, genetic algorithms and random search are prevalent. We refer the reader to Davis (1991) for a review of recent advances in genetic algorithms, and Horst and Tuy (1996) or Zhigljavsky (1991) for theories of global random search. The possible use of such algorithms in conjunction with the model presented here, is currently under investigation by the authors.

References

- Allix, O., Ladevèze, P. and Corigliano, A. (1994), "Damage analysis of interlaminar fracture specimens", *Composites Structures*, Vol. 31, pp. 61-74.
- Bolzon, G. and Corigliano, A. (1997), "A discrete formulation for elastic solids with damaging interfaces", *Comp. Meth. Appl. Mech. Engng*, Vol. 140, pp. 329-59.
- Corigliano, A. (1993), "Formulation, identification and use of interface models in the numerical analysis of composite delamination", *Int. J. Solids Structures*, Vol. 30, pp. 2779-811.
- Davis, L. (1991), *Handbook of Genetic Algorithms*, Thompson Computer Press, Ashington.
- Eustathopoulos, N. and Mortensen, A. (1993), "Capillary phenomena, interfacial bonding and reactivity", in Suresh, S., Mortensen, A. and Needleman, A. (Eds), *Fundamentals of Metal Matrix Composites*, Butterworth-Heinemann, Oxford.
- Hill, R. (1952), "The elastic behaviour of a crystalline aggregate", *Proc. Phys. Soc. (London)*, Vol. A65, pp. 349-54.
- Hill, R. (1963), "Elastic properties of reinforced solids: some theoretical principles", *J. Mech. Phys. Solids*, Vol. 11, pp. 357-72.
- Horst, R. and Tuy, H. (1996), *Global Optimization – Deterministic Approaches*, Springer Verlag, Berlin.
- Huet, C., Navi, P. and Roelfstra, P.E. (1991), "A homogenization technique based on Hill's modification theorem", in Maugin, G.A. (Ed.), *Continuum Models and Discrete Systems*, Vol. 2, Longman, Harlow, pp. 135-43.

-
- Needleman, A. (1987), "A continuum model for void nucleation by inclusion debonding", *J. Appl. Mech.*, Vol. 54, pp. 525-31.
- Needleman, A. (1990a), "An analysis of decohesion along an imperfect interface", *Int. J. Fracture*, Vol. 42, pp. 21-40.
- Needleman, A. (1990b), "An analysis of tensile decohesion along an interface", *J. Mech. Phys. Solids*, Vol. 38, pp. 289-324.
- Needleman, A. (1992), "Micromechanical modeling of interfacial decohesion", *Ultramicroscopy*, Vol. 40, pp. 203-14.
- Needleman, A. Nutt, S., Suresh, S. and Tvergaard, V. (1993), "Matrix reinforcement, and interfacial failure", in Suresh, S., Mortensen, A. and Needleman, A. (Eds), *Fundamentals of Metal Matrix Composites*, Butterworth-Heineman, Oxford.
- Ortiz, M. and Pandolfi, A. (1999), "Finite deformation irreversible cohesive elements for three-dimensional crack-propagation analysis", *The International Journal of Numerical Methods in Engineering*, Vol. 44, pp. 1267-82.
- Ruiz, G., Ortiz, M. and Pandolfi, A. (2000), "Three-dimensional finite-element simulation of the dynamic Brazilian tests on concrete cylinders", *The International Journal of Numerical Methods in Engineering*, Vol. 48, pp. 963-94.
- Zhigljavsky, A.A. (1991), *Theory of Global Random Search*, Kluwer, Dordrecht.
- Zohdi, T.I. and Wriggers, P. (forthcoming), "A model for simulating the deterioration of structural-scale material responses of microheterogeneous solids", *Computer Methods in Applied Mechanics and Engineering* (accepted for publication).
- Zohdi, T.I., Feucht, M., Gross, D. and Wriggers, P. (1998), "A description of macroscopic damage via microstructural relaxation", *The International Journal of Numerical Methods in Engineering*, Vol. 43, pp. 493-507.